Formation of the Rustenburg Layered Suite by assimilation – batch crystallization (ABC) and – fractional crystallization (AFC)

Zhuosen Yao
Department of Earth Sciences, Carleton University, 2115 Herzberg Laboratories, 1125 Colonel By Drive, Ottawa, K1S 5B6, Canada

James Mungall (JamesMungall@cunet.carleton.ca)
Department of Earth Sciences, Carleton University, 2115 Herzberg Laboratories, 1125 Colonel By Drive, Ottawa, K1S 5B6, Canada https://orcid.org/0000-0001-9726-8545

M Jenkins
Department of Earth Sciences, Carleton University, 2115 Herzberg Laboratories, 1125 Colonel By Drive, Ottawa, K1S 5B6, Canada

Article

Keywords:

Posted Date: July 7th, 2020

DOI: https://doi.org/10.21203/rs.3.rs-36556/v1

Version of Record: A version of this preprint was published at Nature Communications on January 21st, 2021. See the published version at https://doi.org/10.1038/s41467-020-20778-w.

Abstract

The Rustenburg Layered Suite (RLS) of the Bushveld Complex of South Africa is a vast layered accumulation of mafic and ultramafic rocks. The layers are widely assumed to result from fractional crystallization from a melt-dominated magma chamber. We derive compositions of all units of the RLS with thermodynamic models of assimilation of crust by a komatiitic parent magma. Ultramafic U-type cumulate layers represent crystal mush produced by single stages of assimilation-batch crystallization (ABC). Anorthositic (A-type) magma mushes emerged by a second stage of batch crystallization during ascent of melts supernatant to mid-crustal U-type cumulates. Only the ferrobasaltic magma of the Upper and Upper Main Zone formed via classical assimilation-fractional crystallization (AFC) and ponded in a melt-dominated magma chamber that subsequently evolved by fractional crystallization. Mineral deposits associated with reversals between mafic and ultramafic layers, hitherto attributed to magma chamber processes, might form in small intrusions entirely lacking melt-dominated magma chambers.

Introduction

Layered mafic intrusions represent portions of the plumbing systems of many large igneous provinces and are principal repositories of several critically important ore elements, including Cr, Ti, V and the platinum-group elements (PGE)1. Layered mafic intrusions such as the iconic Rustenburg Layered Suite (RLS) of South Africa have historically been considered to represent the solidified remnants of vast liquid-dominated reservoirs of magma called magma chambers where crystallization-differentiation has occurred by fractional crystallization2–3. However, an emerging consensus in igneous petrology views large magmatic systems as being dominated by interconnected bodies of mush extending from base to top of the lithosphere and only rarely containing more than a few volume percent of liquid at ephemeral and isolated locations4–6.

The paradigm of magmatic evolution by fractional crystallization (FC) has dominated igneous petrology since Bowen's revolutionary advances a century ago7, subject to recognition half a century later of the importance of crustal assimilation to result in the process of assimilation - fractional crystallization (AFC)8. The fundamental processes driving the evolution of magma composition in AFC are dissolution of host rock or xenoliths, accompanied by cooling and crystal growth, and the immediate removal of crystals from the possibility of continued reaction with the melt (Fig. 1a). Given that AFC is explicitly defined as a fractional process, it is inherent in all AFC models that the system at any given time is composed almost exclusively of melt, into which infinitesimal amounts of contaminant may be titrated, and out of which infinitesimal amounts of solids must be removed due to gravitational sinking. This conceptual underpinning naturally forces the postulate that magmatic evolution occurs within large, liquid-dominated melt reservoirs in the crust (i.e., magma chambers) and drives petrologists to search for the existence of the solidified remnants of such bodies in the rock record. A quintessential small example of closed-system FC-AFC processes is the Skaergaard Intrusion of East Greenland2,9; however, the assumption that large layered mafic intrusions must therefore also represent the solidified remnants of

vast open chambers filled with melt is a reflexive model-driven extension of these ideas that has faced some recent challenges10–13.

A simple conceptual alternative to AFC is that of assimilation in conjunction with the textbook process of batch, or equilibrium, crystallization (i.e., ABC; Fig. 1b). Although the conceptual differences between fractional and equilibrium crystallization may appear arbitrary and purely academic, they describe fundamentally different processes when translated into large-scale magmatic systems. In the simplest expression of this concept, during ABC a magma becomes progressively more contaminated by the ongoing dissolution of wall rock or xenoliths; a hypothetical isenthalpic contamination drives the continuous crystallization of an increasing load of suspended solids which may remain broadly at equilibrium with the enclosing melt via intracrystalline chemical diffusion given sufficient time14. As the proposed reason for FC, the scenario of gravitational sinking of dense solids in static magmas7 does not universally hold true in magmatic systems, i.e., crystallizing phases may not separate from a magma with high viscosity caused by crystallization and SiO_2- enrichment; heat exchange and crystallization in assimilation provide destabilizing buoyancy fluxes to drive forcefully disordered convection of mafic magma, where solids can be passively advected by vigorous convection instead of sinking15; and dense crystals may remain in suspension in most turbulent komatiite flows16. Although equilibrium may not be attained at moderate temperatures, it is likely to occur rapidly in ultramafic magmas17. The success of a hypothetical dimensionless thermodynamic black box ABC process has been demonstrated numerous times, reproducing the observed compositions of ultramafic cumulate rocks and their supernatant magmatic liquids in intrusions both large and small10, 18- 20.

A logical place to test the applicability of the ABC process to igneous petrogenesis at large scales is the Rustenburg Layered Suite (RLS) of South Africa (Fig. 2). Although much has been written about the genesis of the RLS, there is no single published model that seeks simultaneously to account quantitatively for the petrogenesis of all of its constituent units.

Here we propose forward models that recreate the observed bulk rock, mineral, and isotopic compositions of all major constituents of the entire RLS. The spectrum of cumulate rocks observed in the RLS can be described as the products of magma evolution during processes ranging from simple ABC in the ultramafic rocks of the Lower Zone and Critical Zone, through a two-stage ABC process to generate the mafic rocks of the Upper Critical and Main Zones, to classical AFC to form the parental melt for the Upper and Upper Main zones, which then evolved by FC in an essentially closed magma chamber affected by a small number of recharge events.

Results

Application to the Rustenburg Layered Suite, SA

The Paleoproterozoic (~2.056 Ga10, 24) RLS is the world's largest layered mafic intrusive complex, containing ~600,000 km^3 of mafic-ultramafic cumulates and extensive reserves of platinum-group elements (PGE), chromium and vanadium that dominate global resources of these elements21. The RLS

intruded the 2.6–2.3 Ga sedimentary Pretoria Group and 2.061 Ga felsic lavas of the Rooiberg Group at upper crustal levels (~0.06–0.24 GPa)21, 25. In conjunction with the overlying Rashoop Granophyre and Lebowa Granite Suites, they together constitute the Bushveld Complex, comprising an enormous bimodal continental large igneous province in the Kaapvaal Craton (Fig. 2). The closest exposed analogues of Kaapvaal middle crust beneath the RLS are Archean basement amphibolite- to granulite- facies trondhjemitic-granodioritic-granitic gneisses, orthogneisses and metasedimentary rocks exposed in the Vredefort impact structure near Johannesburg26 and in the Southern Marginal Zone (SMZ) of the Limpopo belt to the north of the RLS27.

The RLS is shaped like a dinner plate about 7–9 km thick and ~400 km in diameter (Fig. 2), with moderately inward-dipping marginal zones and flatter-lying central portions. Based on lithological and geochemical investigations, the RLS is traditionally subdivided into five major and laterally continuous stratigraphic zones (Fig. 2)2, 21, 28: (1) the fine- grained, noritic to komatiitic Marginal Zone, which flanks the other zones outside the main layered series and includes a Basal Zone encountered only in drill core beneath the other zones29, (2) discontinuous trough-like bodies of ultramafic Lower Zone (*LZ)* comprising harzburgite, orthopyroxenite and minor dunite interlayers, (3) pyroxenitic Lower Critical Zone (*CZL)* and noritic Upper Critical Zone (*CZU)*,, defined by the occurrence within both of them of prominent and laterally extensive chromitite and sulfide-bearing layers locally enriched in PGE, (4) gabbronoritic Main Zone (*MZ)*,, (5) uppermost ferrogabbroic-noritic and dioritic Upper Zone (*UZ)* with abundant magnetite layers (Fig. 2). Moreover, the *MZ* is sub- divided into the Upper (*MZU)* and Lower MZ (*MZL)* via a prominent, 3 m-thick orthopyroxenite which marks a significant change of initial Sr isotopic ratios (($^{87}Sr/^{86}Sr$)*i)* [23,28.] The *UZ* is also sub-divided into three subzones by the first appearances of magnetite (*UZa)*,, olivine (*UZb)* and apatite (*UZc)* (Fig. 2)[30–31]. It is worth noting that this broad zonal classification is oversimplified for its regional-scale utility, while the cumulate layers show numerous and complex mesoscale variations in their spatial distribution, e.g., intricate details of the lithological macrolayering in *LZ, CZL* and *CZU (*Fig. 2) which cannot be correlated regionally despite the apparent regional correlations implicit in the naming conventions used for the chromitite layers within them32. If the implicit regional correlation of the chromitites is correct, then its regional-scale uniformity is superimposed on a patchwork of locally variable layered cumulate rocks.

The overall stratigraphy of the RLS can be fitted into a two-stage pattern23 assuming that layers were deposited in sequence from bottom to top. The formation of the lower portion from *LZ* to *MZL* has been referred to as the integration stage (Fig. 2), recording multiple influxes and extreme oscillations of dramatically different magmas at the scale of individual macrolayers metres to tens of metres thick, as evidenced both by magmatic unconformities and sharp changes in lithology21, 33, and by the distribution of radiogenic isotopes, exemplified by ($^{87}Sr/^{86}Sr$)*i* 23. This is most clearly expressed in the *CZU* where anorthosite and norite locally alternate with harzburgite, pyroxenite and chromitite at scales of several metres. However, zircon within these contrasting macrolayers has been shown in some cases not to have crystallized in a sequence younging upward through the stratigraphic column, an observation that has called into question the notion of a continuously upward aggrading crystal pile at the base of a

long-lived magma chamber10, 12, 33–34. The formation of the upper portion has been referred to as the differentiation stage (Fig. 2)23, recording relatively uniform parentage as shown by marked uniformity of radiogenic isotope ratios and trace element abundances against a backdrop generally considered to record a well-defined process of fractional crystallization in a large liquid-filled magma chamber with very few magma recharge events28, 31, 35–36, although some recent studies also attributed it to emplacements of several batches of magmas with constant isotopic compositions30, 37. The boundary between the integration stage and the fractionation stage is marked by the pyroxenite marker layer at the base of the *MZU (*Fig. 2), and the resulting composite upper body postulated to have crystallized from a large, quiescent magma body can be termed the “Upper and Upper Main Zone”, or *UUMZ.*

It has been presumed that the mafic sills of the Marginal Zone represent samples of the “parental” magmas that generated the RLS3, 25, 38. Cumulate rocks in the complex can be subdivided into plagioclase-rich mafic units that have been postulated to be crystallization products of tholeiitic magmas referred to as A-type magmas and ultramafic units that have been postulated to be products of high-MgO magmas referred to as U-type magmas39. The U- type magmas contained ~12 to 14 wt.% MgO, corresponding to quench-textured norites exposed in the Marginal Zone surrounding the *LZ* and *CZL* and referred to as the *B1* marginal sills (Fig. 2)25, 38, 40. However, the most primitive olivine and orthopyroxene observed in *LZ* cannot be crystallized from the melts with the composition of the recognized *B1* magma21, 41, and the newfound Basal Ultramafic Sequence beneath the Marginal Zone requires a komatiite as the true parental magma29. The Bushveld U-type magmas are compositionally similar to modern boninites formed by hydrous melting of metasomatized upper mantle38, but Barnes40 proposed a better analogue in the siliceous high magnesium basalts derived from the crustal contamination of komatiites in Archean greenstone belts.

The A-type magmas, thought to have contained ~7–8 wt.% MgO, are tentatively correlated with fine-grained gabbronorites of the Marginal Zone where it abuts the *CZU* and MZL, respectively termed the *B2* and *B3* tholeiitic magmas (Fig. 2)[38–39]. The origins of the A- type magmas have had less attention than that of the U-type, with most investigators apparently assuming that they are commonplace tholeiitic basaltic magmas somehow derived from the upper mantle. Since the mantle does not directly produce tholeiites containing such low MgO contents there must have been some processing of their parental magmas, though this process has not been clearly defined in the past1. *B2* and *B3* are also unconvincing parental magmas due to their partial cumulate characteristics and discrepant crystallization order compared to their interpreted cogenetic cumulates in the RLS21, 25. The bulk composition of the lower portion of RLS is too rich in compatible elements including Cr and the PGE to represent the composition of a liquid42 —it is necessarily regarded as being composed of cumulates deposited from larger volumes of through-going magma that are not presently exposed within the RLS.

The bulk composition of the parental magma that was injected to form the *UUMZ* was proposed by adding ~15–25% of a hypothetical missing segregated component into a weighted average *UUMZ* bulk composition, to form a basaltic andesite with ~5–6 wt.% MgO, but a modeled fractional crystallization sequence from this magma does not closely resemble the natural occurring cumulates28, 36.

Recently discovered spinifex olivine margins chilled at the base of *LZ* strongly argue for a komatiitic parent magma that underwent assimilation of the quartzitic floor22, 29. From this perspective, the remarkable similarities of trace-element features have led to suggestions that the *B1* and *B2–3* magmas were derived from komatiite via > ~40% contamination by upper and lower crust, respectively10, 22, 25. Sr- and Nd-isotopic data of cumulates were used to support the proposition that primitive melt assimilated ~15–30% partial melt of upper crust produce the *LZ* and *CZL,* whereas ~40–50% contamination with the depleted restite in staging chamber beneath RLS is required for the *CZU* and *MZ*[43]. Cr-enrichment and cyclic compositional reversals in the *LZ* have been attributed to episodic influxes of crystals+liquids slurries derived from komatiite contaminated by 20% crust at 4.5–10 kbar42. Consideration of the Cr budget during chromitite formation indicates that the parental liquids must have been komatiitic10, 20, 42. Contamination in deep-seated chambers before final crystal-slurry-type emplacement into the RLS was also proposed on the basis of stable and radiogenic isotope systems27, 44.

In contrast to the various suggestions of crustal contamination, radiogenic 187Os/186Os of sulfide[45] and unradiogenic εHf of zircon from RLS[46] have been used to suggest that the parental magmas were derived from ancient eclogite-bearing subcontinental lithospheric mantle (SCLM) without extensive crustal assimilation. A role for refractory SCLM was also proposed as a possible explanation for the exceptionally high Pt/Pd of Bushveld U-type magmas and mineral deposits47, but it must also be noted that a large degree of melt production is highly unlikely from relatively cool and previously melt-depleted SCLM48.

Since the alleged SCLM Os isotopic signature could equally well be derived from crustal contaminants49, and melt-rock reaction by asthenospheric melts while they pass through refractory SCLM might affect PGE distributions, in the balance we favor the idea that the massive and very short-lived injection of magma that formed the RLS resulted from rapid melting of an asthenospheric mantle plume.

Considering the need for a komatiitic parental magma for the RLS, we suggest that rather than representing samples of the magmas parental to the RLS, the sills preserved in the Marginal Zone may instead be samples of magma that had already passed through the complex, depositing layered cumulate rocks within the RLS before their eventual expulsion into the surrounding Pretoria Supergroup10. Regarding the marginal zone magmas as the complements to the cumulate rocks rather than as their parents alleviates some of the more serious mass balance concerns.

Thermodynamic modeling

To test the applicability of ABC and AFC to the petrogenesis of the RLS, we have modeled the processes using alphaMELTS thermodynamic software50, supplemented by models of isotopic mass balance constrained by the alphaMELTS results. The working hypothesis was that it might be possible to produce representatives of each cumulate rock type preserved as individual macrolayers in the RLS by ABC processes. We chose to model average compositions for each of several key lithologies (Fig. 3) on the

assumption that grain sorting on the macrolayer or hand specimen scale led to much of the observed scatter about the mean values20.

We have considered two distinct scenarios to address the possible origins of the “integration stage” cumulates beneath the base of the UUMZ and a third for the UUMZ, illustrated in Figure 3. In Scenario 1, following the one-stage ABC approach we have already successfully applied to several ultramafic suites worldwide10, 18–20, komatiite is combined with a crustal assimilant in an isenthalpic process, creating a relatively cooler equilibrated mixture of liquid and crystals which then undergoes some degree of cooling while remaining internally at equilibrium. Given the extreme low viscosity (~0.05–0.2 Pa·s), ascent rate as great as m/s and high liquidus temperature (>1550°C) of komatiite16, its emplacement into cooler host rocks (~200–300°C) approximates to forced turbulent convection, where solids are passively advected by chaotic flow and remain in suspension (Fig. 1b)15–16. This stage represents a single batch process of assimilation and cooling during transport through the lithosphere. The mixture is then separated by gravity into a cumulate comprising mostly solids and some trapped liquid, and a supernatant magma comprising mostly liquid and some entrained solids51. This next stage represents the intrusion of the mixture into a sill-like body at the level of the RLS and the resulting dumping of most of the entrained crystal load to form a macrolayer, with internal layering analogous to the stratifications of suspended sediment in water in upper plane bed flow regimes. These successive sill-like magma pulses can be vertically stacked to build up a thick layered pluton based on field observations, geophysical data and numerical models52. Hence, the model cumulate in this stage is compared with ultramafic cumulate rocks of the RLS, and the supernatant magma leaving the system is compared with B1 marginal sill compositions.

In Scenario 2, representing two successive batch steps, it is assumed that a first ABC process occurs in the mid-crust, after which the supernatant liquid rises and undergoes a second batch crystallization as it cools and is emplaced at the level of the RLS to form a mushy macrolayer (Supplementary Fig. 2). During emplacement, this new batch of crystals and melt then separates into cumulate comprising mostly solids and some trapped liquid to represent part of the RLS, and a supernatant magma comprising mostly liquid carrying some entrained crystals that can be compared with the marginal sills. Compositions of solids, liquids, cumulates and marginal sills are shown in Figure 3c, d. This second scenario is therefore a sequence of two batch equilibrium processes which allows for the separation of hidden cumulates from the bulk mixture prior to magma ascent and deposition of the cumulate layer in the RLS—it might be considered as the first step along a continuum of possible process toward AFC.

In Scenario 3, the assimilation and batch removal of crystals occur in a large number of small steps (e.g., 20 to 50 steps) that approximate to AFC as classically understood, presumably occurring within a complex lower-crustal magma reservoir that may have comprised multiple interconnected sill- and dike-like bodies largely composed of mush4–6.

Liquid that has been processed through this AFC mush zone is extracted and emplaced into a large sill-like magma chamber where it subsequently evolves by fractional crystallization, subject to some

subsequent magma replenishment events during the formation of *UUMZ*31.

The parameters used in the models are provided in Supplementary Tables 1–4.

Compositions of endmember magmas, contaminants, solids, liquids, cumulates, and ejected magmas are all shown in Figures 3, 4 and 6. The mantle-derived melt is an Al-undepleted komatiite10. Major and trace element and Sr, Nd, and O isotopic compositions of the magmas and contaminants were estimated by comparison with upper crustal and mid-crustal rocks exposed in the Pretoria Supergroup, Vredefort impact structure, and Limpopo Belt as documented in detail in Supplementary Table 4 and Supplementary Figures 3 and 4.

Ultramafic cumulates of the *LZ, CZL* and *B1* marginal sill compositions were modeled under Scenario 1, assuming an upper crustal assimilant at 0.2 GPa, following a previous Scenario 1 model for the UG2 pyroxenite of the *CZU* and complementary *B1* magma[10]. After assimilation of 17.36% upper crust, *LZ* dunite could form as an adcumulate comprising 4.5% trapped liquid; *LZ* harzburgites require 22.48% assimilation and are modeled as mesocumulates comprising 17.8% trapped liquid, whereas *LZ* and *CZL* pyroxenites could have formed after 27 to 34% assimilation of upper crust to leave a cumulate containing ~15% trapped liquid (Supplementary Table 1 and Supplementary Fig. 1). The *B1* magma is modeled as a mixture of 22% solids equivalent to *CZL* pyroxenite with 78% liquid. The trace- element compositions of these cumulates and B1 marginal sills coincide well with the modeled results (Figs. 4a-b). Because the B1 marginal sills that envelope the *LZ* and *CZL* of the RLS range in thickness from 100–400 m and can penetrate ~100 km into the floor rocks38, their total volume may be regarded as supernatant magmas complementary to emplacement of all of the *LZ* and *CZ* pyroxenites.

Mafic rocks of the noritic portions of the *CZU* and gabbronoritic *MZ* are modeled under Scenario 2, with the same komatiite parent melt but a mid-crustal assimilant at 0.45 GPa. The corresponding temperature of the contaminant was estimated as 390°C via the geothermal model for continental lithosphere and a higher heat flow for the Paleoproterozoic RLS (~70 $mW{\cdot}m^{-2}$) than its current value (51±6 $mW{\cdot}m^{-2}$)[53]. The noritic *CZU* has a xenolith- rich contact sequence with *LZ,* and has widely been regarded as an independent sill-like intrusion of progressive mixtures between B1 and *B2/B3* magmas21, 25. The similar crystallization sequence of *MZL* also requires mixed parental magmas that intrude as crystal slurries from a deeper, staging reservoir after crustal assimilation21. We envision that their primitive komatiites experienced ABC assimilation (~21% for *CZU* and ~24% for *MZL)* and cooled to ~1240–1250ºC in the middle crust to obtain “Bulk 1” compositions (Figs. 3c, d and Supplementary Fig. 2). Retention of ~90–97% of the solids at the site of assimilation left hidden ultramafic cumulates (compositions not shown) in the middle crust with compositions very similar to the *LZ* pyroxenites (Fig. 3). The remaining solids and liquid (“Bulk 2” in Figs. 3c, d and Supplementary Fig. 2) were cooled by conduction during ascent and then separated at the level of the RLS into mafic cumulates and ejected supernatant magmas very similar to the *B2* and *B3* marginal sills. After 40% crystallization at 1181 °C adcumulate norite in the *CZU* contains only 5% trapped liquid; its ejected liquid complement with only 5% solids resembles the *B2* magma apart from the depletion of Rb and Th in the *B2* composition (Figs. 3 and 4c). After 63.9%

crystallization at 1130 °C the modeled *MZL* magma settles to form a mesocumulate containing ~3% trapped liquid and is flanked by marginal *B3* magma that is ejected at a relatively low crystallization degree (~34.2%) and contains ~42% solids (Figs. 3 and 4d). Relative slow cooling and accumulation of crystals may further work on the *B3* rocks that are coarser grained than *B1–2* and have the lowest trace-elements concentrations (Fig. 4).

Scenario 3 is applied to the genesis of the UUMZ. The occurrence of numerous titanomagnetite layers within UUMZ (Fig. 2) indicate that the incoming parental magma was iron-rich28, 36, and hence mafic lower crust is favored as the assimilant54. We suggest that slow rates of introduction of primitive magma into hot lower crust (assumed as 770ºC at 1 GPa due to the heat flow of ~70 mW·m–2) after passage of the vast volumes of magma that produced the Main Zone, combined with muted temperature gradients, might have permitted efficient crystal separation during ongoing crustal assimilation15 (Fig. 1a), in contrast to the vigorous forced convection that favored crystal entrainment during formation of U-type magmas at shallow depth. We modelled the genesis of the parental magma of the *UUMZ* (Fig. 3) by a process of 43.5% AFC contamination in the lower crust plus a further 24% fractional crystallization (FC) during slow upward ascent. After emplacement of this magma in the upper crust, the observed paragenetic sequence and mineral modes of the cumulate rocks (except possible liquid-immiscibility-induced titanomagnetite28, 55) can be reproduced via a closed-system FC model until ~21% melt remains (Fig. 5a). It is debatable whether the final residual liquid was then erupted to form the upper portions of the Rooiberg felsites36, but resolution of this controversy is not material to the success of our models because they focus on magma sources, not on their final residues. Compositional variations of major minerals throughout the *UUMZ* are fitted if the trapped-liquid-driven compositional shift is included (Fig. 5), but also exhibit a series of minor reversals driven by several batches of magma replenishment, which may have resulted in the formation of magnetite layers31, 37.

The largest reversals of plagioclase An% (An45 to An51, Fig. 5b), clinopyroxene $Mg^{\#}$ (~26- 53, Fig. 5c), orthopyroxene $Mg^{\#}$ (~27–42, Fig. 5d) and olivine Fo% (Fo6 to Fo29, Fig. 5e) across the boundary between cycles V and VI, for instance, can be modeled by a small-scale (~1.2%) magma replenishment (Fig. 5).

The isotopic compositions observed in the RLS are compared with the results of our model of transcrustal assimilation and batch or fractional crystallization (Fig. 6). The measured inverse correlation between $(^{87}Sr/^{86}Sr)_i$ and εNd values of RLS (Fig. 6a) are matched well by all models except for the B3 magma, which is represented by very few samples25.

Restricted ranges of $(^{87}Sr/^{86}Sr)_i$ in *B1* vs *B2* and *B3* marginal sills have been widely used to support assertions that these were samples of the U-type and A-type parental liquids of the RLS, but thess observations are equally consistent with our proposition that the sills represent the liquid residues from deposition of the corresponding cumulates (Fig. 6a). High δ18O (average 7.1‰) without apparent systematic changes in RLS is consistent with the isotopic composition of the proposed crustal

assimilants (Fig. 6b), but not with composition of the eclogite-bearing SCLM of Kaapvaal Craton (mode ~5.9‰) which contains some of the most 18O-depleted (<4.5‰) garnets in the global database56.

Discussion And Conclusions

Our results show that the bulk of the RLS below *UUMZ* appears to have been generated by either one-stage or at most, two-stage episodes of batch crystallization and emplacement in their current locations as crystal mushes (Fig. 3). The melts left over from these processes are represented by the marginal sills.

The application of the ABC concept to magmatic systems in lieu of AFC requires a fundamentally different perspective on the physical form of the magmatic systems in space and time. For crystals to be able to re-equilibrate continuously with the melt during ABC it must be very hot, tending to favor the process in ultramafic magmas but less so in mafic magmas. Furthermore, they must remain suspended and the melt must be well-mixed; both conditions require that the system is undergoing vigorous convection15 and/or turbulent flow16. Free, smooth convection cannot accomplish this. The free magma convection in a hot sill emplaced between cooler host rocks is sluggish and entirely driven by the descent of cool crystal-laden drips to a stagnant base57–58. Once they reach the cool lower boundary, crystals cannot be re-entrained in the convective flow. Except in the exceptional case that a mafic or ultramafic magma reservoir is being heated from below, the requirement of vigorous stirring instead demands that the process is occurring as forced convection in a dynamic flowing magmatic setting like a network of dikes and sills4–6. Confinement to a dynamic conduit setting therefore also implies that ABC occurs quickly during transit of magma through the lithosphere rather than during quiescent evolution of a large melt-dominated magma chamber. It is implicit in an ABC model that as soon as the magma comes to rest, dense crystals will separate from the melt, arresting the process and forming masses of cumulates at any point where magma velocity slows.

AFC and ABC therefore offer extremely different views on the mechanism of delivery of crystals to layered intrusions and consequently on the mode of formation of the intrusions themselves. In classic AFC models the crystals form slowly in small numbers in cool zones near the margins, either settling2, 7 or remaining in situ58–59, to form layers, whereas in ABC the crystals form rapidly during transit through the lithosphere and are dumped in intrusions as masses that may subsequently undergo some crystal sorting into layers10, 20–21, 60–61. There can be no doubt that both mechanisms operate, exemplified by the record of fractional crystallization in, e.g., the Skaergaard Intrusion2, 58, and that of batch emplacement of heavy crystal loads in, e.g., olivine-rich Hawaiian picrite lavas62. Assembly of a large volume of mush through multiple emplacements of magmas generated by the ABC process is an alternative mechanism for the creation of a thick accumulation of mafic or ultramafic crystal mush that will later be recognized as a layered intrusion. This mechanism crucially does not require the layers to have been emplaced in a younging-upward series at the bottom of a classic magma chamber and accommodates recent geochronological10–11 and field33–34, 63 evidence for out-of-sequence layer formation in major layered mafic intrusions.

Wholesale wall-rock assimilation and thorough internal equilibration is difficult or impossible for multiply-saturated basaltic magmas, in which large degrees of solidification are experienced over small ranges in liquidus temperature. In contrast, hot and primitive MgO-rich magmas like komatiites are able to assimilate relatively fusible crustal rocks, including granitoids, basalts, and common sedimentary rocks, in startling large proportions, because their liquidus surfaces are very steep, aided by the latent heat of fusion liberated by the simultaneous crystallization of large volumes of the mafic minerals olivine and pyroxene 10, 18, 64, especially if the crustal rocks are already hot. This is true regardless whether the process is one of AFC or ABC. A typical komatiite melt with as little as 18 wt% MgO can assimilate masses of crustal rock exceeding 50% of its original mass, generating a mass of cumulus olivine and pyroxene approximately equal in mass to the original mass of assimilant 10, 18, 64. The resulting contaminated magma will therefore comprise approximately one third ultramafic solids and two thirds low-MgO basaltic liquid. This solid fraction is well within the range of mobile crystal suspensions that can travel through the crust with essentially Newtonian rheology and density lower than most crustal rocks65. The assimilation process occurs so easily that uncontaminated komatiites are rare and it works to prevent the existence of superheated magmas, which cannot fail to react with and dissolve their containers of host rock. Meanwhile, the extremely high temperatures and low viscosities of komatiites easily drive fast ascent and turbulent flow during emplacement, in which the dense crystals remain in suspension and at equilibrium with the host magma16 —approximating to the conceptual ABC model. It is especially noteworthy that modal proportions of cumulus minerals in ultramafic cumulates such as olivine-chromite or olivine-orthopyroxene mixtures in layered mafic intrusions generally do not conform to the instantaneous modal proportions expected during fractional crystallization, positively requiring that many such cumulates were deposited and mechanically sorted into layers from polyphase suspensions that were broadly at internal equilibrium20, 66. The common occurrence of granular harzburgites (i.e., olivine- orthopyroxene cumulate rocks) and pyroxene-chromite cumulates are explicitly forbidden during fractional crystallization by the peritectic relations among olivine, orthopyroxene, and chromite but are entirely consistent with equilibrium phase relations.

As our modeling of the *UUMZ* indicates, our goal here is not to argue that AFC and FC are not valid petrogenetic processes, but instead to demonstrate that the idealized ABC concept represents a process sufficient to account for much of the spectrum of rock types observed in the world's premier layered mafic intrusion, especially those world-class mineral deposits that are hosted by ultramafic macrolayers, and therefore cannot be ignored.

Furthermore, in those cases where cumulates of contaminated magmas display modal proportions departing from expected cotectic proportions, some form of ABC must be accepted as having occurred. Indeed, a batch process is directly implied by several previous assertions that emplacement of the basal series dunites and granular harzburgites29, *CZ* chromite-bearing pyroxenites42, and *MZ* gabbronorites21 must have involved deposition of thick mushy layers, but these previous studies did not explore the implication that their mushy emplacement models are fundamentally inconsistent with AFC processes.

The implications for the mechanism of formation of layered mafic intrusions by injection of crystal mushes are far-reaching because the emplacement of each batch of magma, to form each macrolayer, is entirely independent from all of the other batches. Even in the Peridotite Zone of Stillwater Complex, which is the type locality for cyclic units representing the idealized products of FC, no evidence can be found for genuine cyclicity due to FC processes20. The ABC process does not require a large magma chamber to explain the sequence of rock types or to account for the lack of cyclicity; neither is the hypothetical existence of a magma chamber denied. We can consider layered mafic intrusions as products of numerous separate intrusive events in a long-lived magma column dominated by mushy zones punctuated by rare events when liquid-dominated magmas are transported and emplaced4–6, 52. Macrolayers do not need to have formed in a younging sequence from bottom to top, although they might have. The hypothesis of mixing of fresh U-type magmas into resident A-type magmas of uncertain provenance to account for sharp reversals in mineral assemblages is not necessary, and the apparently random sequence of mafic and ultramafic layers in the *CZU* can be regarded as the consequence of injection of crystal-rich magma batches that experienced different paths through the lithosphere either a) in the observed stratigraphic sequence or b) out of stratigraphic sequence—either scenario is consistent with the observed occurrence of alternating mafic and ultramafic layers. Emplacement of one mushy macrolayer into still-hot older cumulates that may or may not remain partially molten need not produce easily recognizable chilled margins10, 66.

A profound implication for ore genesis is that the chromitite and sulfide reef deposits in macrolayers of the RLS may each represent one relatively small batch of magma. These small batchs would equally well have formed smaller intrusions containing conduit-hosted chromitites like those of the Ring of Fire, Ontario, Sukinda, India, or Finland or PGE-rich sulfide deposits like the Lac Des Iles Pd deposit of Ontario that occur in intrusions with irregular morphology but rock types effectively identical to those observed in the RLS19, 67. Recognition that the processes involved do not require the existence of a vast magma chamber would open many new areas to exploration for these deposits of critically important strategic metals, areas previously overlooked purely because they do not contain layered mafic intrusions like the RLS.

Methods

Isenthalpic assimilation simulations were carried out using the AlphaMELTS software, version 1.9. We collected the major oxide contents of country rocks (Supplementary Fig. 3) and the closest exposures of middle crust (Supplementary Fig. 4) beneath the RLS, and identified potential representatives of the complex lithological association in this region (Supplementary Table 3). Estimated composition of granulite terrains from the interior of the North China Craton is considered as the assimilant at lower crust levels54. Based on similarities in major oxides, the trace element compositions of upper- and middle-crustal contaminants (Supplementary Table3) are mostly assumed according to the global average values of upper continental crust68 and Archaean grey gneisses69, respectively. Initial enthalpies and phase assemblages of these crustal assimilants are estimated under the suitable pressure-temperature conditions (upper crust, 0.2 GPa, 300°C; middle crust, 0.45 GPa, 390°C; lower crust, 1 GPa, 770°C).

Incremental crustal material was added to the system, and an isenthalpic calculation employs entropy maximization to solve for thermodynamic equilibrium between silicate liquid and solid phases at constant pressure. Any resultant crystals can be equilibrated with or discarded from residual liquid (ABC or AFC, respectively), and the remaining system becomes the starting point for next increment of assimilation. Following wholesale crustal assimilation at mid- (0.45 GPa) and lower-crustal levels (1 GPa), further cooling of ascending magmas in the conduit was represented by an isobaric crystallization at 0.2 GPa at the fayalite-magnetite-quartz solid oxygen buffer.

Variable rare-earth element partition coefficients of clinopyroxene/melt and feldspar/melt were calculated based on lattice strain theory, while constant partition coefficients for remaining elements and melt-solid pairs were taken from a comprehensive work50. Since slight differences in Gibbs free energy among various candidate model pyroxenes may confuse the choice of the second pyroxene after orthopyroxene, we corrected the pyroxene/melt partition coefficients when the algorithm improperly termed a high-Ca clinopyroxene as the second orthopyroxene in the *B3*-Gn (*MZ)* lineage.

Based on evolution model of depleted mantle at 2050 Ma, the $(^{87}Sr/^{86}Sr)_i$ and Nd of mantle- derived magma are calculated as 0.7016 and 3.97, respectively. The δ18O of an uncontaminated mantle-derived magma is widely considered as 5.7‰ in light of the global range of 5.4–6.0‰ in fresh MORB glasses (Korolev et al., 2018). $(^{87}Sr/^{86}Sr)_i$ and Nd values of MC and LC are the averages of extensive collected data in this region (Supplementary Table 4). Limited to rare data of sedimentary Pretoria Group, the O isotopic data of UC is assumed mainly with reference to the overlying Rooiberg Group and adjacent dolomite.

Pretoria Group rocks have higher δ18O (~9–15‰) than the averages of overlying volcanites (7.36‰), granophyres (6.6‰) and granites (7.35‰), and a moderate value (9.6‰) was set for the upper crustal materials (Supplementary Table 4). Average δ18O values of the Vredefort Dome and Limpopo belt mostly fall in the range from 9–10‰, but we adopted a slightly larger δ18O for MC assimilant (10.6‰) assuming a possible greater contribution from δ18O- enriched metapelites. The proposed LC has moderate $Mg^{\#}$ and SiO2/Al2O3 ratios, corresponding to the features of intermediate-type lower crustal granulite xenoliths that has an average δ18O of 9.2‰70.

References

1. Naldrett, A. J. Secular variation of magmatic sulfide deposits and their source magmas. *Geol.* **105**, 669-688 (2010).
2. Wager, L. R. & Brown, G. M. Layered igneous rocks. Oliver & Boyd, Edinburgh London, p. 588 (1968).
3. Davies, G., Cawthorn, R. G., Barton Jr, J. M. & Morton, M. Parental magma to the Bushveld Complex. *Nature* **287**, 33-35 (1980).
4. Cashman, K. V., Sparks, R. S. J. & Blundy, J. D. Vertically extensive and unstable magmatic systems: A unified view of igneous processes. *Science* **355**, eaag3055 (2017).

5. Jackson, M. D., Blundy, J. & Sparks, R. S. J. Chemical differentiation, cold storage, and remobilization of magma in the Earth's crust. *Nature* **564**, 405-409 (2018).
6. Sparks, R. S. J., Annen, C., Blundy, J. D., Cashman, K. V., Rust, A. C. & Jackson, Formation and dynamics of magma reservoirs. *Phil. Trans. R. Soc. A* **377**, 20180019 (2019).
7. Bowen, N. L. The evolution of the igneous rocks. Oxford University Press, London, UK, p. 332 (1928).
8. DePaolo, D. J. Trace element and isotopic effects of combined wallrock assimilation and fractional crystallization. *Earth Planet. Sci. Lett.* **53**, 189-202 (1981).
9. Stewart, B. W. & DePaolo, D. J. Isotopic studies of processes in mafic magma chambers: II. The Skaergaard Intrusion, East Greenland. *Mineral. Petrol.* **104**, 125-141 (1990).
10. Mungall, J. E., Kamo, S. L., McQuade, S. U-Pb geochronology documents out-of- sequence emplacement of ultramafic layers in the Bushveld Igneous Complex of South Africa. *Commun.* **7**, 13385 (2016).
11. Wall, C. J., Scoates, J. S., Weis, D., Friedman, R. M., Amini, M. & Meurer, W.P. The Stillwater Complex: Integrating zircon geochronological and geochemical constraints on the age, emplacement history and crystallization of a large, open-system layered intrusion. *Petrol.* **59**, 153-190 (2018).
12. Robb, S. J. & Mungall, J. E. Testing emplacement models for the Rustenburg Layered Suite of the Bushveld Complex with numerical heat flow models and plagioclase geospeedometry. *Earth Planet. Sci. Lett.* **534**, 116084 (2020).
13. Hepworth, L. N., Daly, J. S., Gertisser, R., Johnson, C. G., Emeleus, C. H. & O'Driscoll, B. Rapid crystallization of precious-metal-mineralized layers in mafic magmatic systems. *Geosci.* **13**, 375-381 (2020).
14. Costa, F., Dohmen, R. & Chakraborty, S. Time scales of magmatic processes from modeling the zoning patterns of crystals. *Mineral. Geochem.* **69**, 545-594 (2008).
15. Höink, T., Schmalzl, J. & Hansen, U. Dynamics of metal-silicate separation in a terrestrial magma ocean. *Geophys. Geosyst.* **7**, Q09008 (2006).
16. Huppert, H. E. & Sparks, R. S. J. Komatiites I: eruption and flow. *Petrol.* **26**, 694- 725 (1985).
17. Jollands, M. C., Zhukova, I., O'Neill, H. St. C & Herman, J. Mg diffusion in forsterite from 1250-1600 °C. *Mineral.* **105**, 525-537 (2020).
18. Mungall, J. E. Crustal contamination of picritic magmas during transport through dikes: the Expo Intrusive Suite, Cape Smith Fold Belt, New Quebec. *Petrol.* **48**, 1021-1039 (2007).
19. Mungall, J. E. *et al*. Eagle's Nest: A magmatic Ni-sulfide deposit in the James Bay Lowlands, Ontario, Canada. In Goldfarb R. J. *et al.* (eds) The challenge of finding new mineral resources: global metallogeny, innovative exploration, and new discoveries- volume II: Zinc-Lead, Nickel-Copper-PGE and Uranium, 539-557 (Society of Economic Geologists Special Publication, 2010).
20. Jenkins, M. C. & Mungall, J.E. Genesis of the Peridotite Zone, Stillwater Complex, Montana, USA. *Petrol.* **59**, 2157-2190 (2018).

21. Maier, W. D., Barnes, S. J. & Groves, D.I. The Bushveld Complex, South Africa: formation of platinum-palladium, chrome- and vanadium-rich layers via hydrodynamic sorting of a mobilized cumulate slurry in a large, relatively slowly cooling, subsiding magma chamber. *Deposita* **48**, 1-56 (2013).
22. Maier, W. D., Barnes, S. J. & Karykowski, B. T. A chilled margin of komatiite and Mg-rich basaltic andesite in the western Bushveld Complex, South Africa. *Mineral. Petrol.* **171**, 57 (2016).
23. Kruger, F. J. The Sr-isotopic stratigraphy of the western Bushveld Complex. *Afr. J. Geol.* **97**, 393-398 (1994).
24. Zeh, A., Ovtcharova, M., Wilson, A. H. & Schaltegger, U. The Bushveld Complex was emplaced and cooled in less than one million years – results of zirconology, and geotectonic implications. *Earth Planet. Sci. Lett.* **418**, 103-114 (2015).
25. Barnes, S. J., Maier, W. D. & Curl, E. A. Composition of the marginal rocks and sills of the Rustenburg Layered Suite, Bushveld Complex, South Africa: Implications for the formation of the platinum-group element deposits. *Geol.* **105**, 1491-1511 (2010).
26. Lana, C., Gibson, R. L., Kisters, A. F. M. & Reimold, W. U. Archean crustal structure of the Kaapvaal craton, South Africa – evidence from the Vredefort dome. *Earth Planet. Sci. Lett.* **206**, 133-144 (2003).
27. Harris, C., Pronost, J. J. M., Ashwal, L. D. & Cawthorn, R. G. Oxygen and hydrogen isotope stratigraphy of the Rustenburg Layered Suite, Bushveld Complex: Constraints on crustal contamination. *Petrol.* **46**, 579-601 (2005).
28. Tegner, C., Cawthorn, R. G. & Kruger, F.J. Cyclicity in the Main and Upper Zones of the Bushveld Complex, South Africa: Crystallization from a zoned magma sheet. *Petrol.* **47**, 2257-2279 (2006).
29. Wilson, A. H. A chill sequence to the Bushveld Complex: Insight into the first stage of emplacement and implications for the parental magmas. *Petrol.* **53**, 1123-1168 (2012).
30. Ashwal, L. D., Webb, S. J. & Knoper, M. W. Magmatic stratigraphy in the Bushveld Northern Lobe: continuous geophysical and mineralogical data from the 2950 m Bellevue drillcore. *Afr. J. Geol.* **108**, 199-232 (2005).
31. Yuan, Q., et al. Pulses of plagioclase-laden magmas and stratigraphic evolution in the Upper Zone of the Bushveld Complex, South Africa. *Petrol.* **58**, 1619-1644 (2017).
32. Scoon, R. N. & Teigler, B. Platinum-group element mineralization in the critical zone of the western Bushveld Complex: I, sulfide poor-chromitites below the UG-2. *Geol.* **89**, 1094-1121 (1994).
33. Mitchell, A. A. & Scoon, R. N. The Merensky Reef at Winnaarshoek, Eastern Bushveld Complex: A primary magmatic hypothesis based on a wide reef *Econ. Geol.* **102**, 971-1009 (2007).
34. Mitchell, A. A. & Scoon, R. N. The Platreef of the Bushveld Complex, South Africa: A new hypothesis of multiple, non-sequential magma replenishment based on observations at the Akanani project, North-West of Mokopane. *Afr. J. Geol.* **115**, 535-550 (2012).
35. Kruger, F. J., Cawthorn, R. G. & Walsh, K. L., 1987. Strontium isotopic evidence against magma addition in the Upper Zone of the Bushveld Complex. *Earth Planet. Sci. Lett.* **84**, 51-58 (1987).

36. Vantongeren, J. A., Mathez, E. A. & Kelemen, P.B. A felsic end to Bushveld differentiation. *Petrol.* **51**, 1891-1912 (2010).
37. Scoon, R. N. & Mitchell, A. A. The Upper Zone of the Bushveld Complex at Roossenekal, South Africa: Geochemical stratigraphy and evidence of multiple episodes of magma replenishment. *Afr. J. Geol.* **115**, 515-534 (2012).
38. Sharpe, M. R. & Hulbert, L. J. Ultramafic sills beneath the Eastern Bushveld Complex: Mobilized suspensions of Early Lower Zone cumulates in a parental magma with boninitic affinities. *Geol.* **80**, 849-871 (1985).
39. Irvine, T. N., Keith, D. W. & Todd, S. G. The J-M platinum-palladium reef of the Stillwater Complex, Montana: II, Origin by double-diffusive convective magma mixing and implications for the Bushveld Complex. *Geol.* **78**, 1287-1334 (1983).
40. Barnes, S.J. Are Bushveld U-type parent magmas boninites or contaminated komatiities? *Mineral. Petrol.* **101**, 447-457 (1989).
41. Yudovskaya, M. A., Kinnarid, J. A., Sobolev, A. V., Kuzmin, D. V., McDonald, L. & Wilson, A. H. Petrogenesis of the lower zone olivine-rich cumulates beneath the platreef and their correlation with recognized occurrences in the Bushveld Complex. *Geol.* **108**, 1923-1952 (2013).
42. Eales, H. V. & Costin, G. Crustally contaminated komatiite: primary source of the Chromitites and Marginal, Lower, and Critical Zone magmas in a staging chamber beneath the Bushveld Complex. *Geol.* **107**, 645-665 (2012).
43. Maier, W. D., Arndt, N. T. & Curl, E. A. Progressive crustal contamination of the Bushveld Complex: evidence from Nd isotopic analyses of the cumulate rocks. *Mineral. Petrol.* **140**, 316-327 (2000).
44. Roelofse, F. & Ashwal, L. D. The Lower Main Zone in the Northern Limb of the Bushveld Complex – a >1.3 km thick sequence of intruded and variably contaminated crystal mushes. *Petrol.* **53**, 1449-1476 (2012).
45. Richardson, S. & Shirey, S.B. Continental mantle signature of Bushveld magmas and coeval diamonds. *Nature* **453**, 910-913 (2008).
46. Zirakparvar, N. A., Mathez, E. A., Scoates, J. S. & Wall, C. J. Zircon Hf isotope evidence for an enriched mantle source for the Bushveld Igneous Complex. *Mineral. Petrol.* **168**, 1050 (2014).
47. Mungall, J. E. & Brenan, J. M. Partitioning of platinum-group elements and Au between sulfide liquid and basalt and the origins of mantle-crust fractionation of the chalcophile elements. *Cosmochim. Acta* **125**, 265-289 (2014).
48. Yao, Z. S., Qin, K. Z. & Mungall, J. E. Tectonic controls on Ni and Cu contents of primary mantle-derived magmas for the formation of magmatic sulfide deposits. *Mineral.* **103**, 1545-1567 (2018).
49. Day, J. M. D. & O'Driscoll, B. Ancient high Pt/Os crustal contaminants can explain radiogenic 186Os in some intraplate magmas. *Earth Planet. Sci. Lett.* **519**, 101-108 (2019).
50. Smith, P. M. & Asimow, P. D. Adiabat_1ph: A new public front-end to the MELTS, pMELTS, and pHMELTS models. *Geophys. Geosyst.* **6**, Q02004 (2005).

51. Rice, A. & Moore, J. M. Physical modeling of the formation of komatiite-hosted nickel deposits and a review of the thermal erosion paradigm. *Mineral.* **39**, 491- 503 (2000).
52. Annen, C., Blundy, J. D., Leuthold, J. & Sparks, R. S. J. Construction and evolution of igneous bodies: Towards an integrated perspective of crustal magmatism. *Lithos* **230**, 206-221 (2015).
53. Jones, M. Q. W. Heat flow in the Bushveld Complex, South Africa: implications for upper mantle structure. *Afr. J. Geol.* **120**, 351-370 (2017).
54. Gao, S., *et al*. Chemical composition of the continental crust as revealed by studies in East China. *Cosmochim. Acta* **62**, 1959-1975 (1998).
55. Fischer, L. A., et al. Immiscible iron- and silica-rich liquids in the Upper Zone of the Bushveld Complex. *Earth Planet. Sci. Lett*. **443**, 108-117 (2016).
56. Korolev, N. M., Melnik, A. E., Li, X. H. & Skublov, S. G. The oxygen isotope composition of mantle eclogites as a proxy of their origin and evolution: A *Earth Sci. Rev.* **185**, 288-300 (2018).
57. Bergantz, G. W. & Ni, J. A numerical study of sedimentation by dripping instabilities in viscous fluids. *J. Multiph. Flow* **25**, 307-320 (1999).
58. McBirney, A. R. & Noyes, R.M. Crystallization and layering of the Skaergaard Intrusion. *Petrol.* **20**, 487-554 (1979).
59. Langmuir, C. H. Geochemical consequences of in situ crystallization. *Nature* **340**, 199-205 (1989).
60. Mondal, S. K. & Mathez, E. A. Origin of the UG2 chromitie layer, Bushveld Complex. *Petrol.* **48**, 495-510 (2007).
61. Forien, M., Tremblay, J., Barnes, S. J., Burgisser, A. & Pagé, P., 2015. The role of viscous particle segregation in forming chromite layers from slumped crystal slurries: Insights from analogue experiments. *Petrol.* **56**, 2425-2444 (2015).
62. Baker, M. B., Alves, S. & Stolper, E. M. Petrography and petrology of the Hawaii Scientific Drilling Project lavas: Inferences from olivine phenocryst abundances and compositions. *Geophys. Res.* **101**, 11715-11727 (1996).
63. Mitchell, A. A., Scoon, R. N. & Sharpe, M. R., 2019. The Upper Critical Zone in the Swartklip Sector, north-western Bushveld Complex, on the farm Wilgerspruit 2JQ: Origin by intrusion of ultramafic sills with concomitant partial melting of host norite- anorthosite cumulates. *Geol. Soc. S. Afr.* **122**, 143-162 (2019).
64. Sparks, R. S. J., 1986. The role of crustal contamination in magma evolution through geological time. *Earth Planet. Sci. Lett*. **78**, 211-223 (1986).
65. Yao, Z. S., Mungall, J. E. & Qin, K. Z. A preliminary model for the migration of sulfide droplets in a magmatic conduit and the significance of volatiles. *J Petrol* **61**, egaa005 (2020).
66. Bédard, J. H. J., Marsh, B. D., Hersum, T. G., Naslund, H. R. & Mukasa, S. B. Large- scale mechanical redistribution of orthopyroxene and plagioclase in the Basement Sill, Ferrar Dolerites, McMurdo Dry Valleys, Antarctica: Petrological, Mineral- chemical and field evidence for channelized movement of crystals and melt. *Petrol.* **48**, 2289-2326 (2007).

67. Djon, M. L., Olivo, G. R., Miller, J. D., Peck, D. C. & Joy, B. Stratiform platinum- group element mineralization in the layered Northern Ultramafic Center of the Lac des Iles Intrusive Complex, Ontario, Canada. *Ore Geol. Rev.* **90**, 697-722 (2017).
68. Rudnick, R. L. & Gao, S. Composition of the continental crust. In Turekian, K. K. & Holland, H. D. (eds) Treatise on Geochemistry, Second Editionth edn, vol. **4**, 1-52 (Elsevier-Oxford, 2014).
69. Moyen, J. E. & Martin, H. Forty years of TTG research. *Lithos* **148**, 312-336 (2012).
70. Kempton, P. D. & Harmon, R. S. Oxygen isotope evidence for large-scale hybridization of the lower crust during magmatic underplating. *Cosmochim. Acta* **56**, 971-986 (1992).

Declarations

Author contributions

JEM, ZSY and MCJ developed the ideas and shared initial pilot-scale modeling efforts. ZSY and JEM compiled literature and data sources. ZSY performed the modeling in depth with frequent inputs from JEM and MCJ and produced all the figures and tables. JEM and ZSY wrote the manuscript.

Competing Interests

The authors declare no competing interests.

Figures

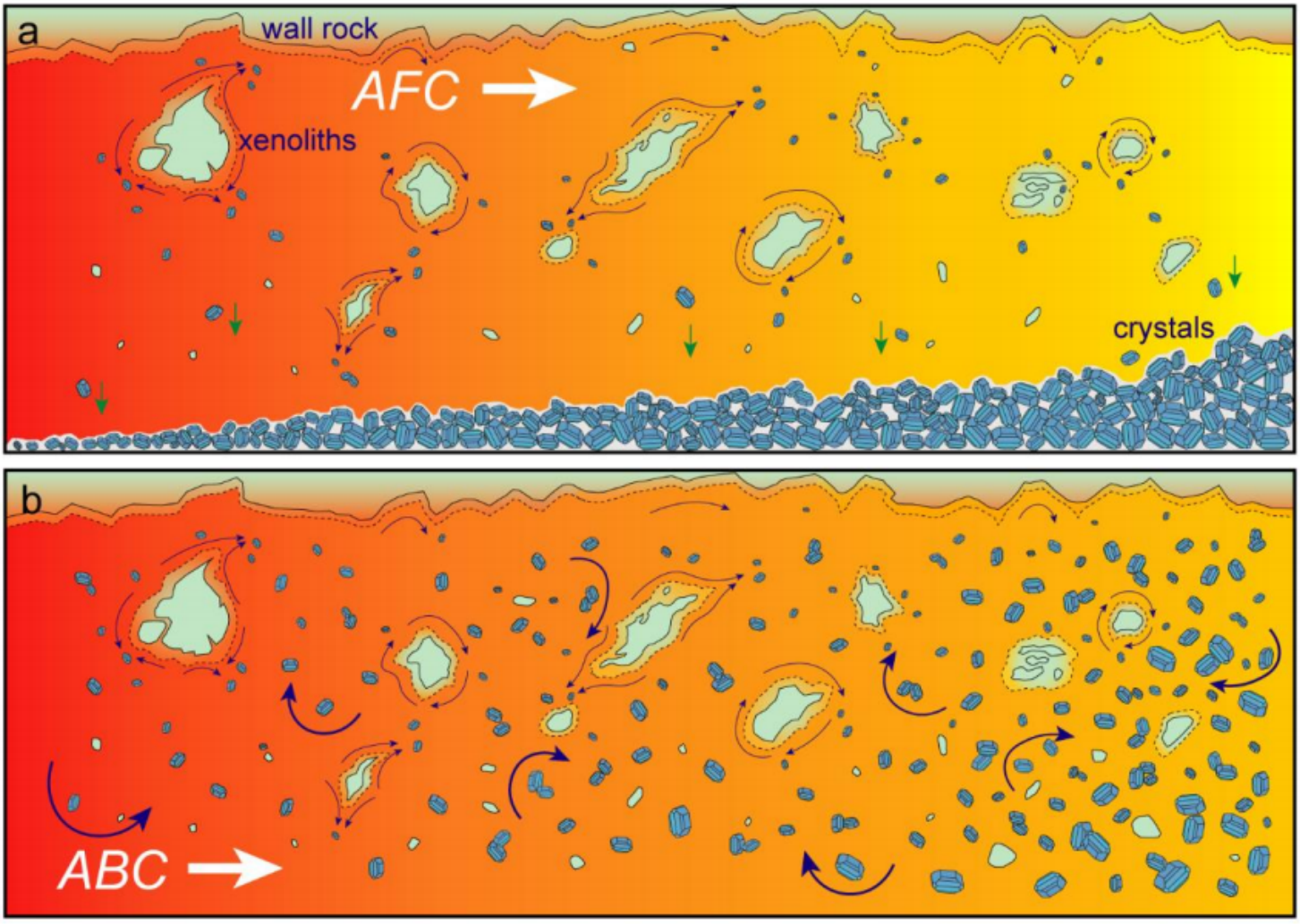

Figure 1

Schematic illustration of temporal evolution of magmas from left to right. Bulk assimilation mostly occurs on the wallrock-magma boundaries via dissolution and/or from the crustal xenoliths induced by magmatic stoping. a. classical AFC model; heat for crustal assimilation is supplemented by concurrent fractional crystallization while newly formed crystals are immediately sequestered from an almost entirely crystal-free liquid. b. in the ABC model, during assimilation a steadily increasing amount of precipitated solids remains suspended by forced convection during magma flow and is continuously re-equilibrated with magma until it comes to rest and the solids are deposited all at once.

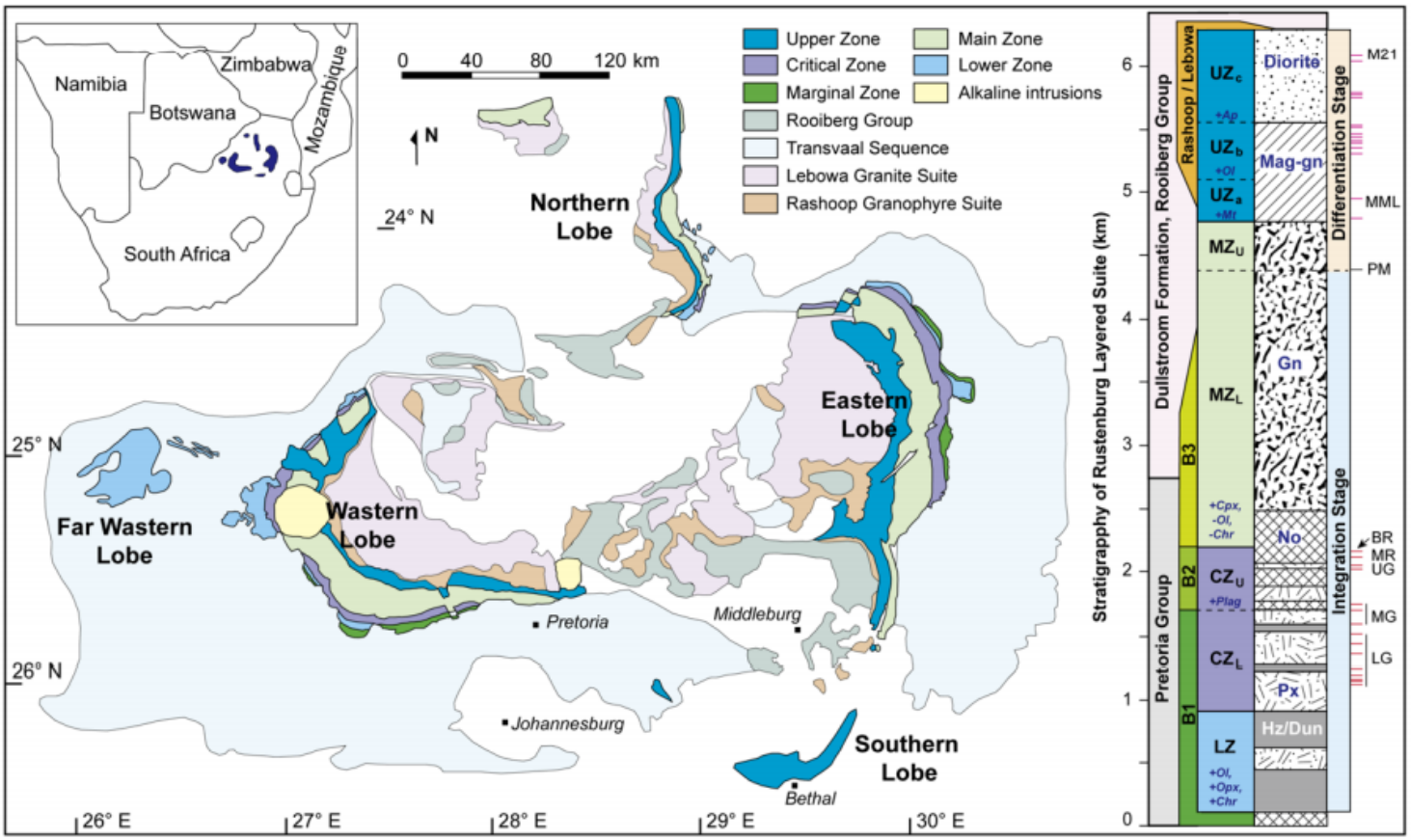

Figure 2

Geological map of the Bushveld Complex and stratigraphic column of the Rustenburg Layered Suite. Adapted from multiple sources cited in the text10, 21-23. Because the RLS is discordant, its position within the host rock series varies from the base of the Pretoria Group in the north to the lower Rooiberg Group in the south. Inset diagram shows the location of the Bushveld Complex within South Africa. Marker horizons: LG, lower group chromitites; MG, middle group chromitites; UG, upper group chromitites; MR, Merensky Reef; BR, Bastard Reef; PM, Pyroxenite Marker; MML, main magnetite layer; M21, magnetite layer 21. Abbreviation: Ol, olivine; Opx, orthopyroxene; Cpx, clinopyroxene; Chr, chromite; Plag, plagioclase; Mt, magnetite; Ap, apatite; Hz, harzburgite; Dun, dunite; Px, pyroxenite; No, norite; Gn, gabbronorite; Mag-gn, magnetite gabbronorite.

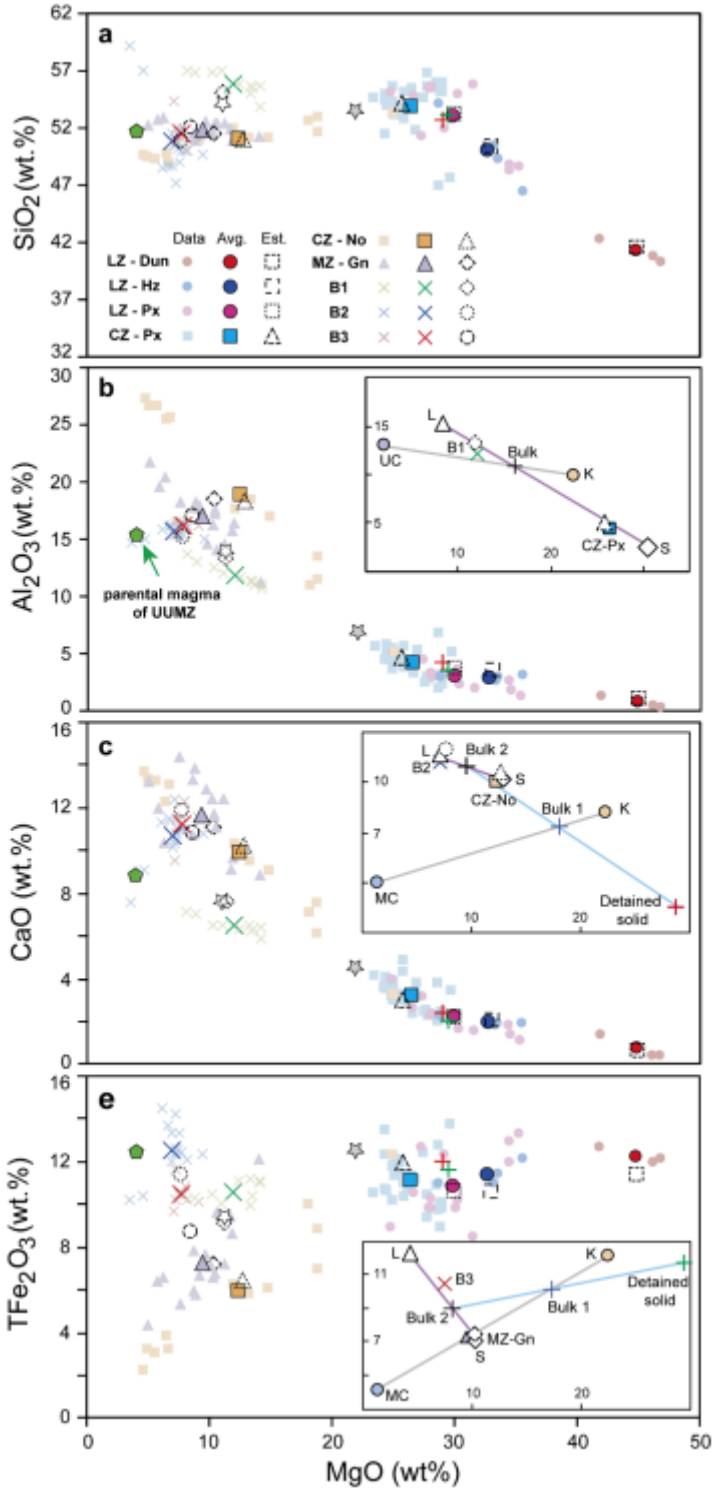

Figure 3

Comparisons of whole-rock geochemical data with the model results. Bivariate diagrams for whole-rock compositions from the lithogeochemical section of RLS21. Compositions of komatiite, upper crust and middle crust are shown as “K”, “UC” and “MC”, respectively. Grey and purple lines represent the komatiite-crust assimilation trends and the solid-liquid reallocation relationship, respectively, in the B1-Px(CZ) lineage (b). Similar relationships exist for each of the ABC processes to generate other LZ and CZ

ultramafic macrolayers (Supplementary Fig. 1). The two-stage ABC processes creating the B2-No (CZ) lineage and B3-Gn (MZ) lineage are illustrated in the insets of panels (c) and (d). A first ABC process generates liquid and solid, and the compositions of solids retained at depth for the B2-No (CZ) and B3-Gn (MZ) lineages are marked as vertical red and green crosses, respectively. Removal of first-stage solids as described in the text generates a new bulk composition ('Bulk 2') that is emplaced in the RLS and crystallized to form the illustrated solid and liquid compositions. Inset diagrams zoom in on the specific area where crystal sorting between model liquid ("L") and solid ("S") would generate the observed cumulates and corresponding phenocryst-bearing marginal rocks. The white and grey stars represent the modeled B1 and UG2 cumulate, respectively, from the one-stage ABC approach of Mungall et al.10. The proposed parental magma for the UUMZ is exhibited as green pentagons, and also shown in the Supplementary Table 3. Abbreviations: Hz, harzburgite; Dun, dunite; Px, pyroxenite; No, norite; Gn, gabbronorite; Ave., average compositions of the corresponding lithologies based on the representative section of RLS from Maier et al.21; Est., estimated compositions derived from the thermodynamic models. All data collected from multiple sources cited in the text21, 25, 30.

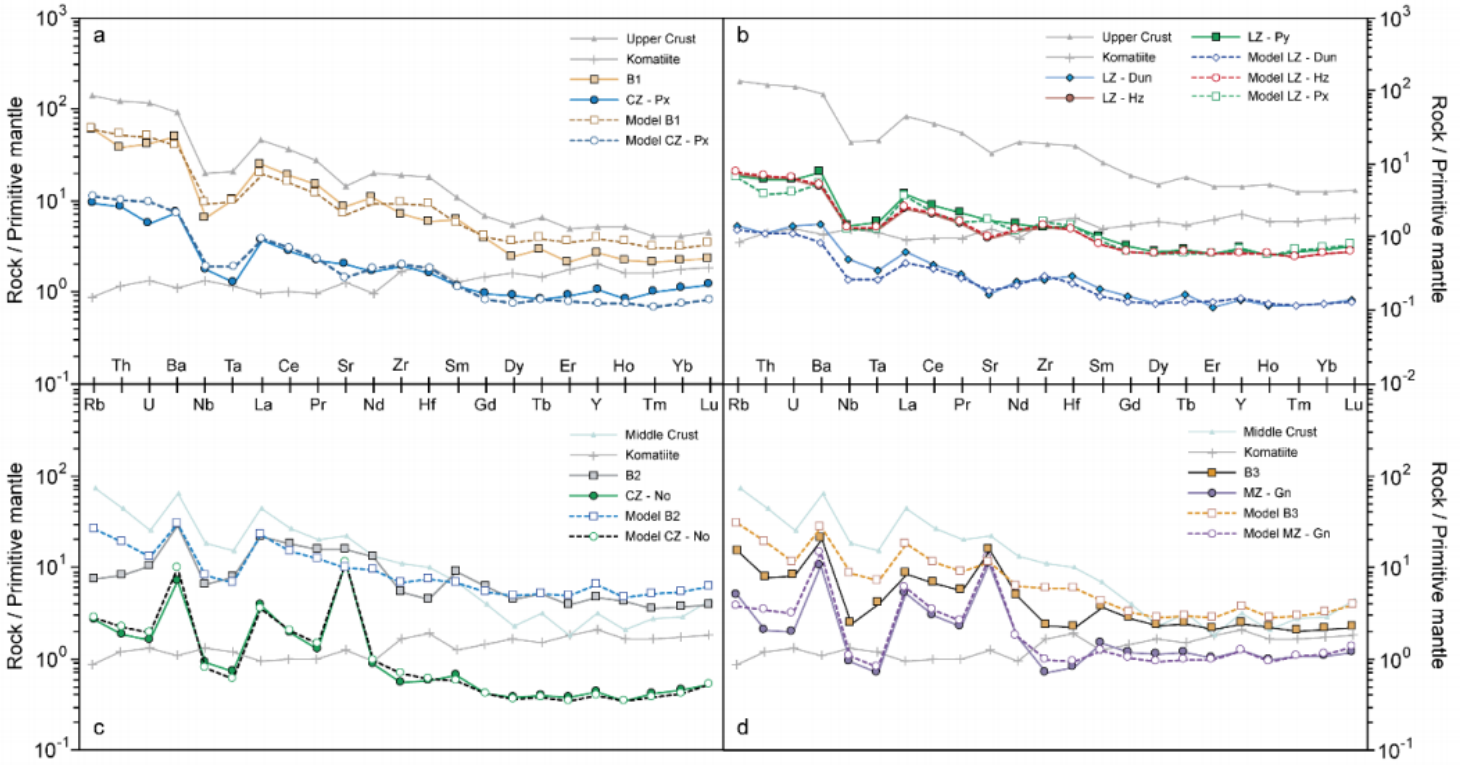

Figure 4

Primitive mantle-normalized trace element concentrations for natural and model rocks from the RLS. Solid symbols joined by solid lines represent averages compositions of rocks from the RLS, while open symbols joined by dashed lines represent alphaMELTS models. Compositions of upper crust, middle crust and komatiite are shown in Supplementary Table 3.

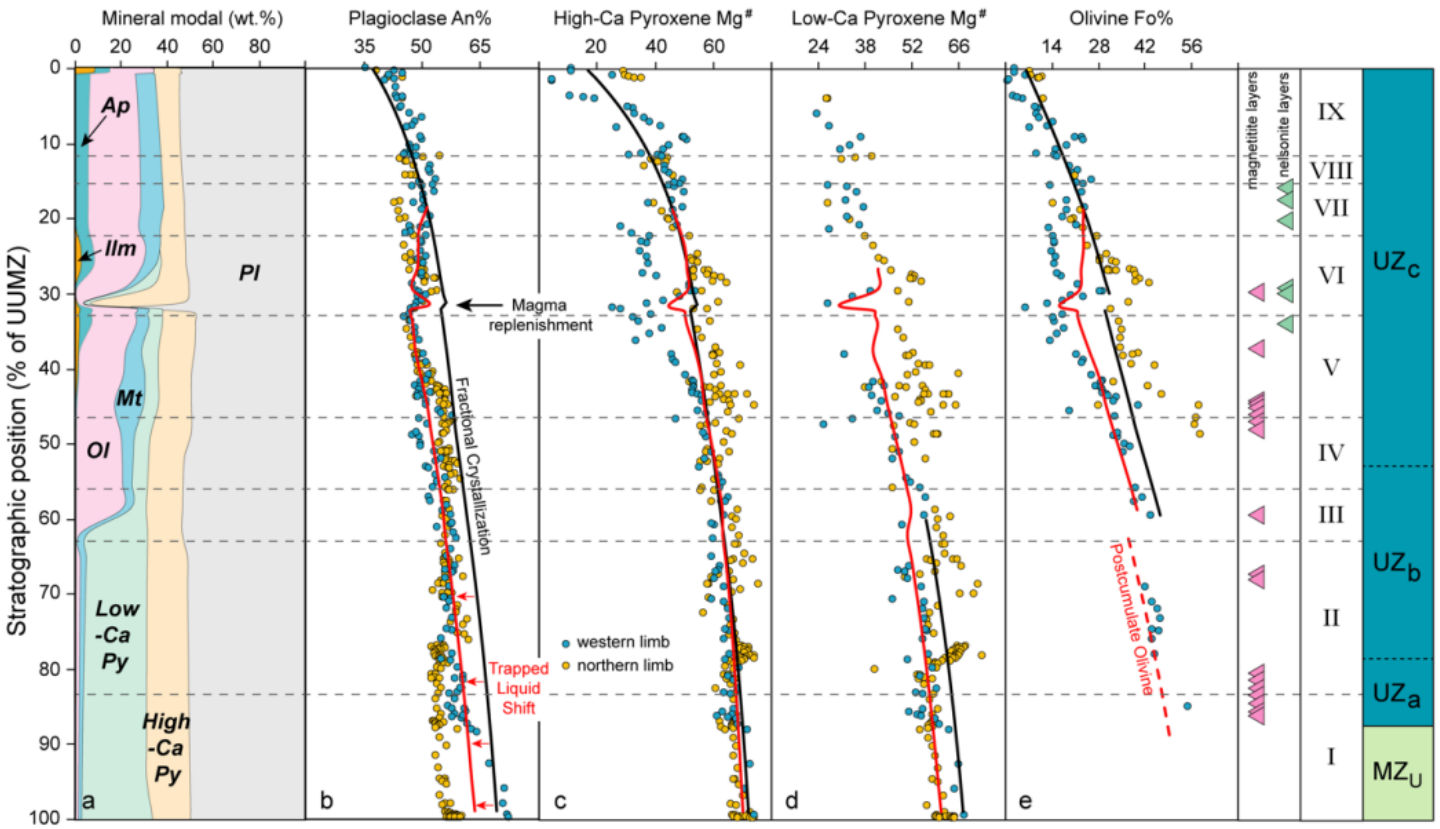

Figure 5

Modal abundances and compositional variations of minerals throughout the UUMZ. a. The predicted mineral modes from AlphaMELTS modelling for the proposed parental magma of UUMZ in Figure 3. Comparisons between the measured composition variations (blue circles from the Bierkraal at the Western Limb28, 31; yellow circles from the Bellevue at the Northern Limb30) and model results of b. plagioclase (An%, 100Ca/(Ca+Na)), c. high-Ca pyroxene (Mg#, 100Mg/(Mg+Fe)), d. low-Ca pyroxene (Mg#) and e. olivine (Fo%, 100 Mg/(Mg+Fe)) with stratigraphic position. Cycles I-VI are identified by marked reversal in An% number of plagioclase from the Bierkraal drill cores, western limb28. A further three cycles (VII-IX) are defined by the disappearance of apatite without apparent reversal in An%, but have still been explained in the same way as cycles I-VI28. The UZ contains ~30 magnetitite and nelsonite (magnetite-ilmenite-apatite cumulate) layers that host world-class V, Ti and P resources. Compositional variations of major minerals crystallized from the incoming parental magma are shown as the black lines, whereas the trapped liquid shifts (red lines) represent compositional modifications of minerals induced by the reduction of trapped interstitial melt fraction from 25% to 5% in the post-cumulate stage. Olivine in cycle II is crystallized in the trapped liquid shift, corresponding to its low modal proportion (~1-2%) and prismatic shape31. Replenishment of ~1.2% initial parental magma at the boundary of cycles V and VI drives apparent reversals of mineral modes and compositions, which coincide with the observed data (reversals in olivine Fo%, pyroxene Mg# and plagioclase An%)28, 31.

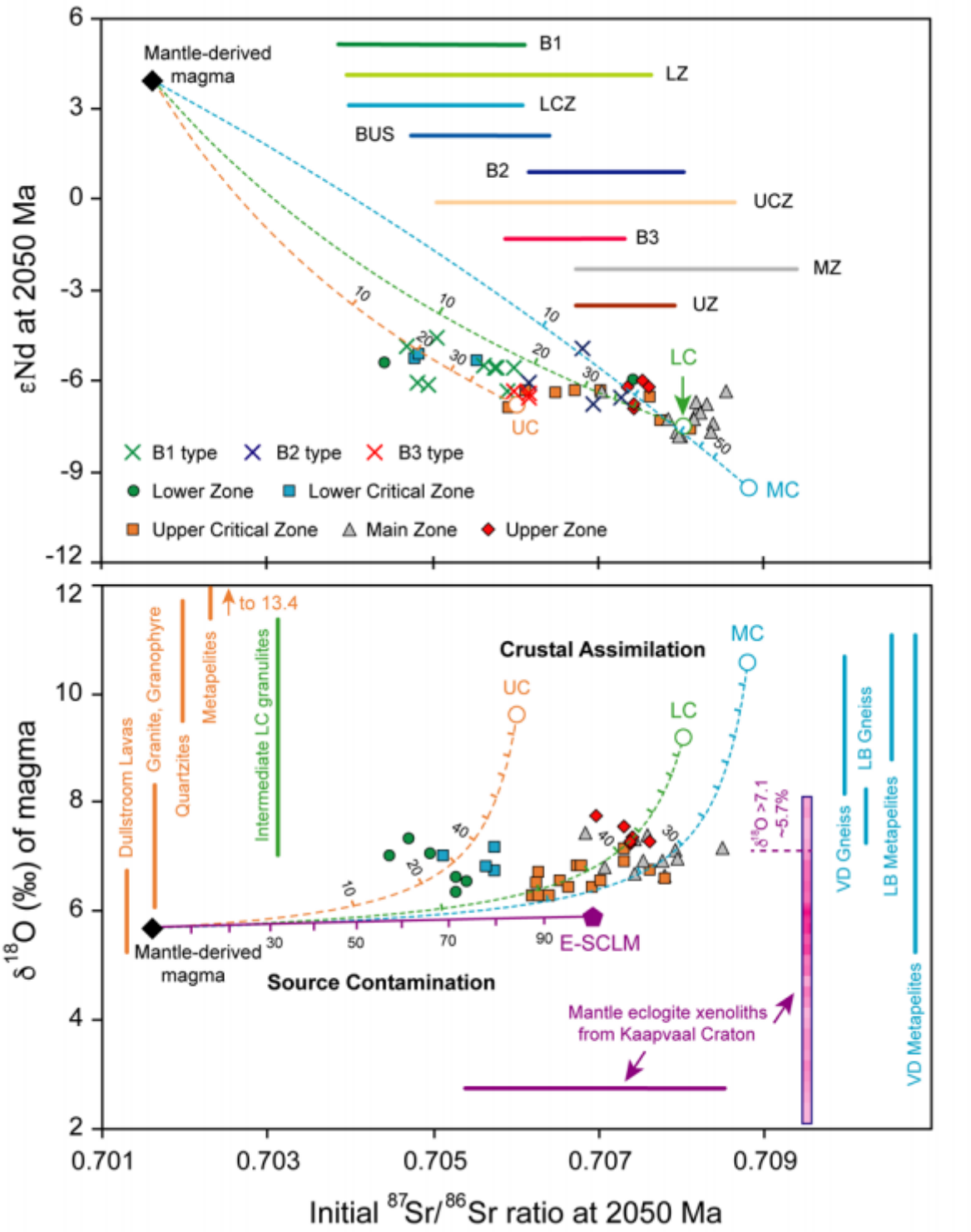

Figure 6

Isotope correlation diagrams comparing RLS rocks to assimilation models. Curves represent modelled assimilation of primary, mantle-derived magma with different end-members from the Kaapvaal Craton: dashed orange line, upper crust; dashed blue line, middle crust; dashed green line, lower crust; purple line, eclogite-bearing SCLM (E-SCLM). a. εNd-(87Sr/86Sr)i. Horizontal bars exhibit (87Sr/86Sr)i ranges in marginal rocks and cumulate zones of RLS. b. δ18O-(87Sr/86Sr)i. δ18O averages with standard

deviations of potential assimilants in upper, middle and lower crusts are shown schematically by vertical orange, blue and green bars, respectively; averages for various contaminants are shown by circles and star. (87Sr/86Sr)i average plus its standard deviation of E-SCLM is exhibited by purple horizontal bar, and δ18O distribution of mantle eclogite xenoliths from the Kaapvaal Carton is shown by vertical pinkish-purple color bar with deep tone corresponding to a higher frequency. Garnets with δ18O>7.1‰ represent ~5.7% of the total 157 samples available from the Kaapvaal Carton56. All data were collected from multiple sources cited in the supplementary references. Abbreviation: LB, Limpopo Belt; VD, Vredefort Dome.

Supplementary Files

This is a list of supplementary files associated with this preprint. Click to download.

- YaoMungallJenkinsNCSupplementaryData.pdf